Journal of Fluorescence (2019) 29:727–735
https://doi.org/10.1007/s10895-019-02393-1

ORIGINAL ARTICLE

A Novel Biscarbazole-Xanthene Hybrid Fluorescent Probe for Selective and Sensitive Detection of Cu^{2+} and Applications in Bioimaging

Kun Huang[1] · Defang Han[1] · Xianglin Li[1] · Mengni Peng[1] · Qi Qiu[1] · Dabin Qin[1]

Received: 7 March 2019 / Accepted: 6 May 2019 / Published online: 19 May 2019

Abstract

A new biscarbazole-fused xanthene hybrid dye **MeBCX** has been prepared by CH_3SO_3H-promoted condensation of 4-hydroxycarbazole and *o*-phthalic anhydride, followed by esterification with methanol, which exhibits good cell membrane permeability. Taking advantage of the spiro-controlled xanthene platform of the dye, a Cu^{2+}-selective fluorescence "off-on" probe **BCX-Cu** has been successfully prepared with excellent performances in selectivity and sensitivity, and the detection limit is calculated to be 88.7 nM. The sensing mechanism is confirmed to involve a specific cascade reactions of Cu^{2+}-induced spirolactam ring-opening and hydrolysis. In addition, living L929 cell imaging demonstrates the probe has living cell membrane permeability and shows great potential for tracing intracellular Cu^{2+} through fluorescence imaging technology.

Keywords Carbazole · Xanthene · Fluorescence · Copper ions · Cell imaging

Introduction

Small organic fluorescent dyes get wide applications in chemosensors and biological imaging [1–6], optical device design [7, 8] and photodynamic therapy [9, 10]. Xanthene dyes, especially rhodamine derivatives attract much concerns in the development of various molecular chemosensors owing to their merits of emission wavelengths higher than 550 nm and featuring controllable spiro-leuco moiety. Taking advantages of the chemically modifiable spiro-ring platform, a large number of fluorescent probes with signal off-on behaviors have been explored because their distinct signal changes compared to the lower fluorescence background signals, which are favorable for the applications in bioimaging [11–20]. On the other hand, carbazole units are well known as an electron-donating substituent groups that have received much concerns in organic light-emitting devices (OLEDs), fluorescent maker and drug synthesis due to its high hole-transporting properties, strong fluorescence emission and excellent pharmacological properties [21–24]. Though a great many of chemosensors have been developed based on carbazole units, so far as know, a limited number of carbazole-xanthene hybrid chemosensors were reported in the field of fluorescence sensing [25]. Therefore, to design and prepare carbazole-xanthene hybrid dyes that may combine their merits for biological application and fluorescent probe design is of great significance and worthy of exploring.

To be an important essential transition metal element, copper plays vital roles in keeping normal functions of several enzymes in human body, including cytochrome *c* oxidase (C*c*O), ceruloplasmin (CP), lysyl oxidase (LOX), Cu/Zn superoxide dismutase (SOD1), dopamine beta-hydroxylase and peptidylglycine alpha-amidating monooxygenase [26]. As we know, the homeostasis of copper in human body is tightly associated with copper transport proteins, for example,

Electronic supplementary material The online version of this article (https://doi.org/10.1007/s10895-019-02393-1) contains supplementary material, which is available to authorized users.

✉ Kun Huang
hkun2017@cwnu.edu.cn

✉ Dabin Qin
qdbkyl@cwnu.edu.cn

[1] Key Laboratory of Chemical Synthesis and Pollution Control of Sichuan Province, School of Chemistry and Chemical Engineering, China West Normal University, Nanchong 637002, People's Republic of China

chaperones and copper transporter 1 (human, hCTR1) [27]. Nevertheless, irregular concentration variation of Cu^{2+} may cause a variety of neurodegenerative diseases probably related to copper, and among which the well-known are Alzheimer's, Menkes and Wilson diseases [28–31]. As mentioned above, investigations on Cu^{2+}-related physiological processes via Cu^{2+}-selective fluorescence probes with the assistance of fluorescence imaging technology are of great significance and have recently received extensive concerns and numerous achievements have been made in bioimaging applications. Since the first example of Rhodamine B based chemosensor has been designed for the detection of Cu^{2+} by utilizing the Cu^{2+}-induced hydrolysis reaction of hydrazide to rhodamine in the 1990s [32], substantial number of chemosensors for Cu^{2+} have been developed with outstanding performances in selectivity and sensitivity [33–56]. However, there is a continuous demand in constructing chemosensors that hold highly selective and sensitive performances in Cu^{2+} ions detection. Hence, to design and synthesize fluorescent off-on probe for Cu^{2+} by using a new fluorophore is still attractive. As mentioned above, as well as a continuous effort for the development of fluorescent probes, we herein reported the synthesis of a biscarbazole-fused xanthene hybrid dye **MeBCX** with good cell membrane permeability and its application in design of a new Cu^{2+}-selective fluorescent probe **BCX-Cu,** a tracer for monitoring Cu^{2+} by living cell imaging.

Experimental

Materials and Equipments

Commercial reagents/solvents obtained via Aladdin (Shanghai, China) were used directly. UV-Vis spectrophotometer (Shimadzu, UV-2550) was used for the measurement of absorption spectra. Fluorescence emission spectra were measured on Cary Eclipse fluorescence spectrophotometer (Varian, Victoria Australia) provided by a Xe lamp and 1.0 cm quartz cells. NMR (400/100 MHz) spectra were recorded on a Bruker Avance II 400 MHz NMR spectrometer and chemical shifts δ were reported in ppm based on internal standard TMS. High resolution mass spectra (HRMS) were recorded on an Agilent 6510 Q-TOF LC/MS instrument (Agilent Technologies, Palo Alto, CA). A X-4 melting-point apparatus with microscope was used to record melting points. pH values were determined by a PHSJ-3F pH meter (Leici, Shanghai, China). Single crystal structure data of **BCX-Cu** was collected by using Bruker SMART APEX-II CCD detector provided with a graphite monochromatic Mo-Kα radiation (λ = 0.71073 Å). Fluorescence imaging images were acquired on a FV 1000-IX81 confocal laser scanning microscope (Olympus, Japan).

Sample Preparation

Stock solutions of **MeBCX/BCX-Cu** (5 mM) were obtained by dissolving them in DMF, respectively. Stock solutions (10 mM) of all metal ions were obtained through dissolving their nitrate salts in distilled water. Test solutions were set up at 5/10 μM by accurately diluting corresponding stock solutions with appropriate solutions. Unless otherwise stated, the optical spectra were recorded in CH_3CN-H_2O (pH = 7.4, v / v, 1 / 1) after 40 min.

Synthesis of MeBCX

4-hydroxycarbazole (3.66 g, 20 mmol) and *o*-phthalic anhydride (1.48 g, 10 mmol) were mixed in CH_3SO_3H (8 mL), stirred and heated at 85 °C for 2 days. As the liquid cooled, it was slowly poured into ice water mixture to produce large amount of precipitation. The precipitate was collected and dried in vacuo for further use without separation. The dry mixture was dissolved in methanol (50 mL) before slowly added concentrated H_2SO_4 (4 mL) in an ice-water bath. Then the resulting solution was heated to reflux for 24 h and most of methanol was removed by evaporation. The residue was neutralized by $NaHCO_3$, extracted with CH_2Cl_2 (40 mL × 3), dried over anhydrous Na_2SO_4 and evaporated to dryness in vacuo, which was purified by column chromatography on silica gel using dichloromethane and methanol (v / v = 20: 1) as elution. An brownish red solid was obtained in the yield of 19.0% (0.93 g), melting point: 202–204 °C. ^{1}H NMR (400 MHz, DMSO-d_6) δ (ppm) 13.09 (s, 1H), 8.70 (d, J = 7.4 Hz, 2H), 8.42 (d, J = 7.9 Hz, 1H), 8.09 (t, J = 7.7 Hz, 1H), 8.00 (t, J = 7.7 Hz, 1H), 7.83 (d, J = 7.7 Hz, 2H), 7.71 (d, J = 7.7 Hz, 3H), 7.56–7.49 (m, 4H), 7.44 (d, J = 7.4 Hz, 2H), 3.40 (s, 3H). ^{13} C NMR (100 MHz, DMSO-d_6) δ (ppm) 166.59, 165.11, 152.02, 147.49, 139.37, 134.43, 133.37, 131.02, 130.97, 129.16, 127.28, 122.62, 121.64, 120.31, 116.37, 115.09, 113.29, 108.93, 52.85. ESI-HRMS: calcd. m/z 493.1552 for $[M + H]^+$, found m/z 493.1540 for $[M + H]^+$,

Synthesis of BCX-Cu

2-hydrazinopyridine (0.46 g, 6 mmol) was added slowly to a stirred solution of **MeBCX** (0.49 g, 1 mmol) in methanol (8 mL) under ambient temperature. The resulting mixture was stirred at 60 °C until large amount of precipitate was observed (ca. 2 h). After cooling, the precipitate was collected and washed with cool CH_3OH, which was purified by column chromatography on silica gel using CH_2Cl_2 and CH_3OH (60: 1) as elution. A white powder was obtained in the yield of 62.0% (0.35 g), melting point: 235–237 °C. ^{1}H NMR (400 MHz, DMSO-d_6) δ (ppm) 11.66 (s, 2H), 8.90 (d, J = 7.6 Hz, 2H), 8.26 (s, 1H), 7.98–7.96 (m, 1H), 7.78 (d, J = 3.9 Hz, 1H), 7.67–7.61 (m, 4H), 7.53–7.44 (m, 4H), 7.27–7.24 (m, 3H), 7.19–7.16 (m, 1H), 6.89 (s, 1H),

6.47–6.44 (m, 1H), 6.28 (d, $J = 8.4$ Hz, 1H). ^{13}C NMR (100 MHz, DMSO-d_6) δ (ppm) 164.92, 158.57, 152.07. 148.01, 147.12, 146.85, 141.13, 139.43, 137.59, 136.74, 133.62, 129.66, 128.89, 125.34, 124.58, 122.78, 121.66, 120.73, 119.21, 117.87, 114.76, 113.95, 111.34, 109.73, 108.24, 107.56, 106.50, 65.89. ESI-HRMS: calcd. m/z 570.1930 for $[M + H]^+$, found m/z 570.1952, 1139.3679 for $[M + H]^+$ and $[2\ M + H]^+$, respectively.

L929 Cells Imaging Using the Dye MeBCX and Probe BCX-Cu

All imaging experiments were conducted by using L929 cells, which were obtained from commercial suppliers and cultured in MEM (modified Eagle's medium) containing 10% FBS and 1% antibiotics in a 5% CO_2 atmosphere at 37 °C. Cells were set in a 96-well plate and cultured for imaging until they plated on glass-bottom. Next, the cells were stained by **MeBCX/BCX-Cu** (1.0/3.0 μM, respectively) for 60 min and washed in PBS. After that, the cells stained by **BCX-Cu** were supplemented with 18.0 μM of Cu^{2+} in the growth medium for 1 h and rinsed three times with PBS, which were then employed for fluorescence imaging.

Quantum Yield

The relative quantum yields (Φ_1) were evaluated using standard reported in literature (rhodamine B: 0.50 in ethanol) [57] according to the same method as employed in Gong et al. (2016) [58].

Results and Discussion

Synthesis

Scheme 1 shows synthesis route of target compounds **MeBCX** and **BCX-Cu**. Firstly, **MeBCX** was prepared by condensation reaction of commercial compound 4-hydroxycarbazole and *o*-phthalic anhydride in CH_3SO_3H at 85 °C for 48 h according the literature [59], The resulting mixture was further esterified without separation by using methanol with a yield of 19.0%. Next, the target compound **BCX-Cu** was obtained at the yield of 62.0% as white power by modifying the carboxyl group of **MeBCX** with commercially available 2-hydrazinopyridine in methanol according to our previous method [36].

Structural Confirmation and X-Ray Diffraction Study

The structures of dye **MeBCX** and chemosensor **BCX-Cu** were determined by using spectroscopic methods including ^{1}H NMR, ^{13}C NMR, and HRMS, and the details were presented in supporting information. The single crystals of **BCX-Cu** was obtained by slow evaporation of its CH_3CN solution at ambient temperature.

X-ray crystallography was used to determine the structure of **BCX-Cu** crystals from the diffusion of its CH_3CN solution. The data were collected at 293(2) K. Crystal data for BCX-Cu.CH_3CN were presented as the follows: monoclinic, space group $P2_1/c$, a = 8.9903(18) Å, b = 37.384(7) Å, c = 9.7527(19) Å, $\alpha = 9.7527(19)°$, $\beta = 113.385(4)°$, $\gamma = 90.00°$, $V = 3008.6(10)$ Å^3, $Z = 4$, $T = 293.(2)$ K, μ (MoKα) = 0.086 mm^{-1}, $D_{calc} = 1.348$ g/cm^3, crystal dimension: 0.20 × 0.18 × 0.30 mm^3, 15,764 reflections measured ($4.358° \le 2\Theta \le 50.698°$), 5511 unique ($R_{int} = 0.0620$, $R_{sigma} = 0.0839$) used in all calculations. 0.0496 ($I > 2\sigma(I)$) and 0.1432 (all data) were obtained for R_1 and wR_2, respectively. The assigned CCDC number of the molecule is 1,885,337. Figure 1 shows the mean plane N5-C25-C26-C27-C28 is nearly perpendicular to the xanthene moiety with a dihedral angle of 89.70 (3)°, which is analogues to the literatures [60]. Meanwhile, the two carbazole rings are not rigidly located on symmetrical position but form a dihedral angle of 8.76 (6)°.

Optical Properties of MeBCX

Absorption and Emission Profiles of MeBCX

The pH stability of **MeBCX** was evaluated in water under different pH (containing 5% methanol, pH 1–12) and the details were provided in supporting information (Fig. S1a). The absorption intensity of **MeBCX** presented obvious spectral signal over a wide pH range of 1–12, only with slight change under highly acidic environment. However, the fluorescence signal kept stable at the pH range of 5–12 and the gradual

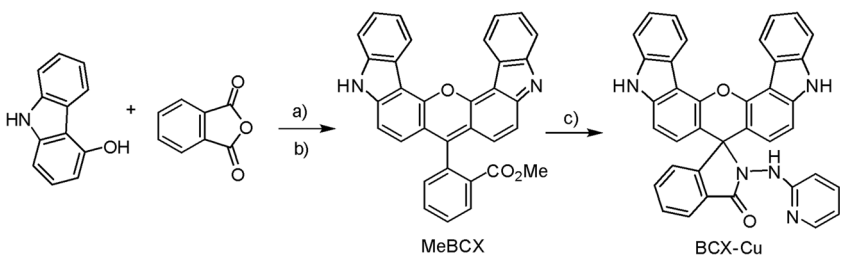

Scheme 1 Procedures for preparation of **MeBCX** and **BCX-Cu**. Reagents and conditions: a) CH_3SO_3H, 85 °C, 48 h; b) Methanol, 2-hydrazinopyridine, 60 °C, 2 h.

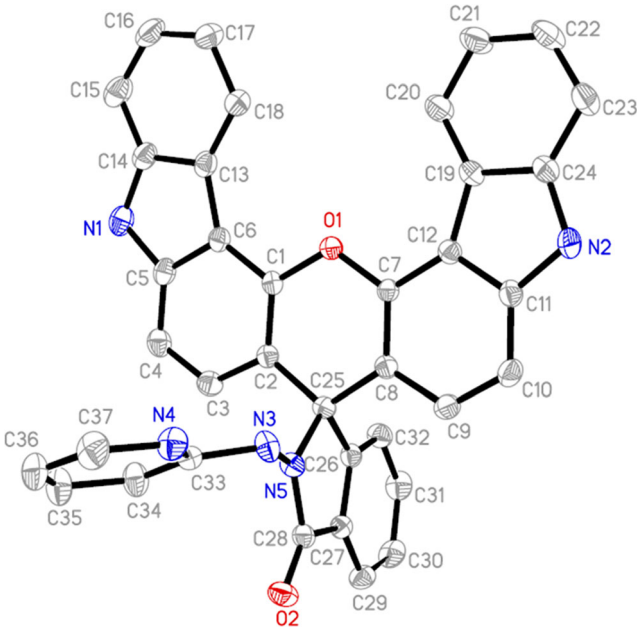

Fig. 1 ORTEP plot of **BCX-Cu** drawn at 50% probability ellipsoids. All H-atoms and CH_3CN-molecule were omitted for clarity. Selected bond lengths (Å) and angles (°): N3 - N5 1.380(3); N1 - N5 1.382(3); C1 - O1 1.388(3); C13 - C6 1.451(4); C13 - C18 1.396(4), N4 - C33 1.332(3); C5 - N1 - C14 109.7(2); N5 - C25 - C2 111.4(2); C1 - O1 - C7 118.53(19); N5 -C25 -C26 99.14(19); N5 - N3 - C33 120.7(2)

decrease of pH value (5–1) would cause the distinct reduce of emission intensity at 520 nm (Fig. S1b), which may ascribe to the structural conversions between protonated cations and neutral molecule **MeBCX** as illustrated in Scheme S1**.** The results indicate **MeBCX** has a good stability over a wide pH range (5–12), and exhibits great potential in biological applications.

The absorption and emission profiles of **MeBCX** in $CHCl_3$, CH_2Cl_2, EtOH, CH_3OH, CH_3CN, H_2O, acetone and THF were recorded respectively. Figure 2a exhibited single absorption bands centered at about 520 nm ($\varepsilon \geq 0.70 \times 10^4$ M^{-1} cm^{-1}) of **MeBCX** in various solvents, which may ascribe to the π-π* electronic transitions in its π-extended framework. Simultaneously, **MeBCX** exhibited the maximum emission centered at ca. 560 nm in different solvents with Stokes shifts ranged from 4 to 62 nm under 480 nm excitation (Fig. 2b). The maximum emission wavelength (λ_{em}) of **MeBCX** gradually increased according to the order of H_2O, MeOH, $CHCl_3$, CH_2Cl_2, EtOH, THF, CH_3CN, acetone with obvious solvatochromism phenomenon. In addition, the quantum yields of **MeBCX** were evaluated in different solvents and moderate quantum yields can be obtained in CH_3CN. The corresponding data were summarized in Table S1.

Fluorescence Imaging by MeBCX

Firstly, cell permeability of the dye **MeBCX** was performed using L929 cells through confocal fluorescence microscope to estimate the potential of **MeBCX** to be a fluorescent tracer for biological applications. As shown in Fig. 3, the cell morphology stained by **MeBCX** (1.0 μM) for 1 h did not change significantly (Fig. 3a). Obvious florescence signals could be seen in the red channel (510–600 nm) with excitation at 488 nm (Fig. 3b). Meanwhile, the merged image suggested the fluorescence signals were distributed in the intracellular regions, confirming the cell permeability of **MeBCX** (Fig. 3c). The results show the promising biological applications of the dye as fluorescence maker.

Recognition Behaviors of BCX-Cu towards Cu^{2+}

Fluorescence and Absorption Behaviors of BCX-Cu for Cu^{2+}

In consideration of the mentioned above as well as to demonstrate the feasibility of **MeBCX** for probe design, a spiro ring closed fluorescent probe **BCX-Cu** for Cu^{2+} has been prepared through modification of the carboxyl group in the hybrid carbazole-xanthene molecule **MeBCX**.

The titration trail of **BCX-Cu** towards Cu^{2+} via absorption and emission spectra were performed in CH_3CN-H_2O (pH = 7.4, v /v, 1 / 1) and Fig. S2 (supporting information) showed **BCX-Cu** (5 μM) exhibited obvious absorption bands at 319 nm and 334 nm, agreeing with the characteristic absorption bands of carbazole moiety [61]. However, no significant absorption band over 400 nm was observed due to a

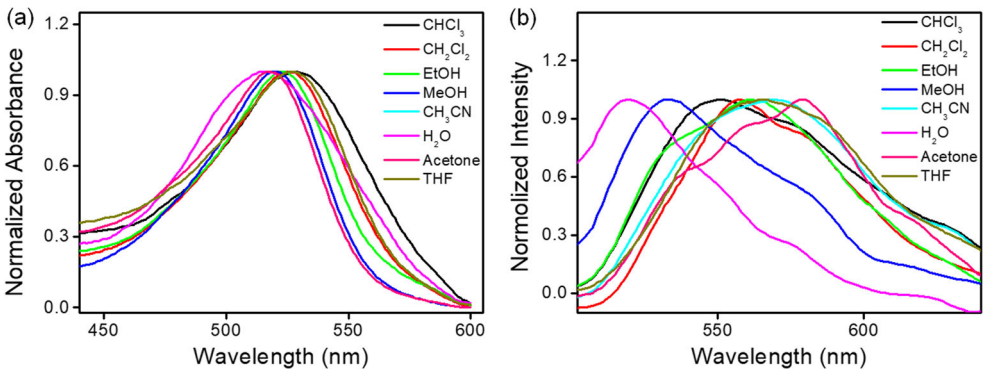

Fig. 2 **a** Absorption and **b** emission profiles of **MeBCX** in various solvents, λ_{ex} = 480 nm; slits: 2.5 nm, 5 nm

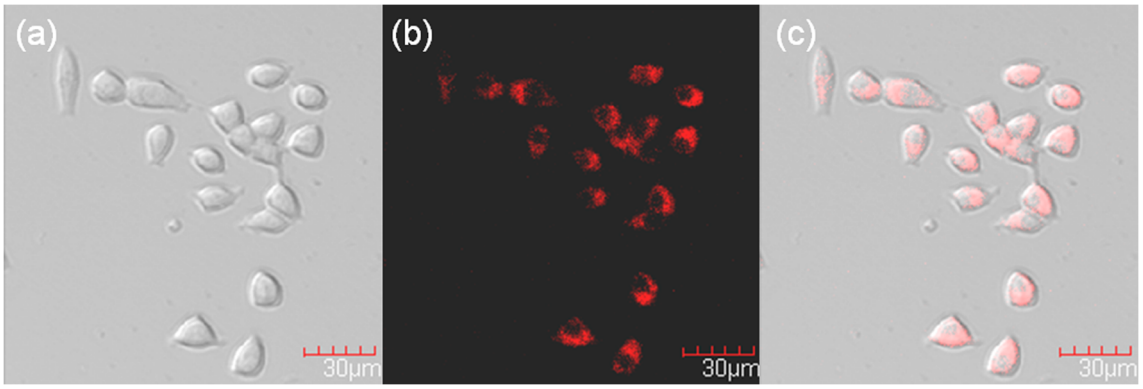

Fig. 3 Fluorescence images of **MeBCX** (1 μM) stained (1 h) L929 cells. **a** Bright field, **b** fluorescence image and **c** merged image, images collected from the range of 510–600 nm upon 488 nm excitation

spirocyclic hydrazide form of the probe **BCX-Cu** in these conditions. As expected, the additions of Cu^{2+} (0–10.0 equiv.) to a solution of **BCX-Cu** elicited an simultaneous emergence in the absorption bands at ca. 536 nm by increasing concentrations of Cu^{2+}, besides, the **BCX-Cu** solution could be observed with visual color transformation as shown in Fig. S3, indicating Cu^{2+} – promoted the spirolactam ring-opening of **BCX-Cu**. The absorbance at 536 nm was almost no more increase when the amount of Cu^{2+} increased to 9.0 equivalents of the probe, and no significant changes was encountered by the further treatment of Cu^{2+}, suggesting the spectra saturation was reached.

Next, the fluorescence titration profiles of **BCX-Cu** in respond to Cu^{2+} were investigated under the above conditions (Fig. 4). At first the probe **BCX-Cu** was observed with very weak fluorescent signals over 520 nm, suggested the formation of a ring-closed circular hydrazide structure in the probe molecule. In contrast, an enhanced emission intensity (570 nm) was observed followed by increasing concentrations of Cu^{2+}. The spectra saturation was reached after the concentration of Cu^{2+} was over 50.0 μM, and no significant fluorescence changes occurred by further additions of Cu^{2+}. According to titration curves of fluorescence, a dissociation constant (K_d) was calculated as $(19.233 \pm 0.385) \times 10^{-6}$ M (correlation coefficient: 0.99936, Fig. S4) [35]. Meanwhile, the LOD (limit of detection) for Cu^{2+} was determined to be 8.87×10^{-8} M according to the formula 3σ/k reported in literature [36] (Fig. S5). The results suggest **BCX-Cu** can be employed as an highly sensitive sensor for Cu^{2+} and presents promising potential in quantitatively monitoring Cu^{2+} in real water samples .

To explore the sensing mechanism of turn-on fluorescence of **BCX-Cu** induced by Cu^{2+}, HRMS and ^{1}H NMR experiments were carried out respectively. Firstly, the fluorescent mixture of **BCX-Cu** in presence of Cu^{2+} (8 equiv.) was recorded through HRMS (Fig. S6). The intense peak at 477.2062 $[M]^+$ (calcd. m/z 477.1245 for $[M]^+$) confirmed the Cu^{2+}-promoted hydrolysis reaction of spirolactam and generation of new fluorescent compound (Scheme 2) [32]. Meanwhile, a weak peak at 570.1924 $[BCX\text{-}Cu + H]^+$ (calcd. 570.1930 $[M + H]^+$) of residual probe molecule was also observed. Subsequently, ^{1}H NMR spectra of **BCX-Cu** titrated with different amounts of Cu^{2+} was recorded. As illustrated in Fig. S7, the addition of Cu^{2+} caused the obvious variations of protons 5–8 in pyridine ring and aromatic protons 1–4 in **BCX-Cu**, which should be ascribed to the Cu^{2+}-promoted structural changes from spirolactam to π-extended spiroring-opening hydrolyzed product. Therefore, Scheme 2 provides a possible proposal for the sensing mechanism of **BCX-Cu** in detection of Cu^{2+}.

It is significant for selective chemosensors to achieve high selectivity in the detection of the target object among various analytes. Thus, the fluorescence profiles were utilized to evaluate the specific response of **BCX-Cu** (10 μM) to Cu^{2+} among other common metal ions in $CH_3CN\text{-}H_2O$ (pH = 7.4, v /v, 1 / 1). Figure 5a clearly indicated the addition of other ion

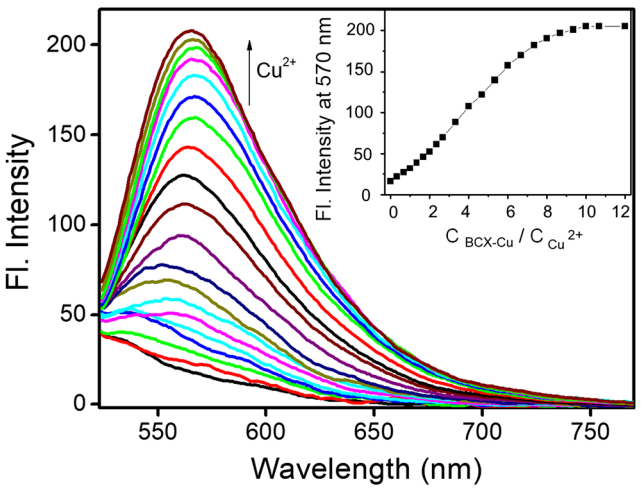

Fig. 4 Fluorescence spectra of **BCX-Cu** (5 μM) with the addition of Cu^{2+} (0–60 μM) in $CH_3CN\text{-}H_2O$ (pH = 7.4, v / v, 1 / 1). Inset: the relationship between emission intensity and $C_{Cu^{2+}}/C_{BCX\text{-}Cu}$, λ_{ex}: 500 nm, slits: 10 nm, 10 nm

Scheme 2 The suggested sensing mechanism of **BCX-Cu** towards Cu^{2+}

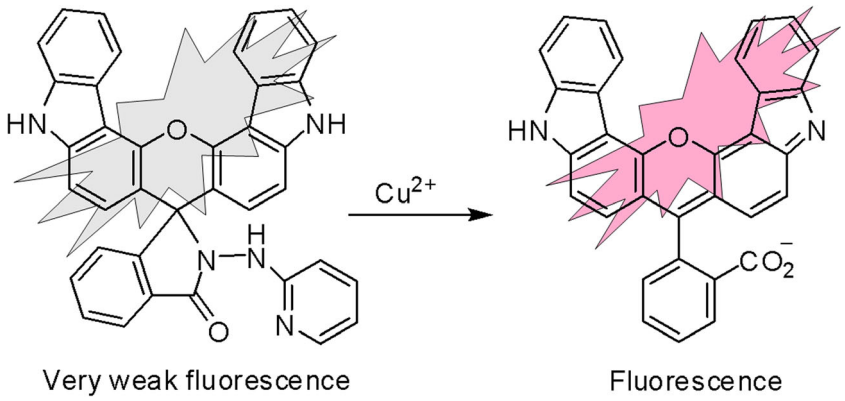

species (6.0 equiv., Ag^+, Al^{3+}, Ba^{2+}, Ca^{2+}, Co^{2+}, Cd^{2+}, Cr^{3+}, Fe^{2+}, Fe^{3+}, Hg^{2+}, K^+, Mg^{2+}, Na^+, Ni^{2+}, Pb^{2+} and Zn^{2+}) did not cause significant changes on emission spectra compared to that of free **BCX-Cu** as well as any appreciable emission intensity changes at 570 nm. While, the addition of equivalent Cu^{2+} triggered a pronounced fluorescence increase of the probe solution at 570 nm with over 10-fold enhancement of fluorescence intensity. Meanwhile, the selectivity of **BCX-Cu** (5 μM) for Cu^{2+} were also evaluated via UV-Vis absorption spectra under the same conditions. As illustrated in Fig. S8, only the presence of Cu^{2+} (6.0 equiv.) can induce a distinct enhancement in absorbance at 536 nm, with a visible change in color from colorless to red. Other ion species induced neglectable variations in color and absorption spectra (Fig. S3). These results demonstrate the probe **BCX-Cu** exhibits high selectivity in the detection of Cu^{2+}.

In consideration of the effect of co-existed metal ions in practical Cu^{2+} sample determination, the competition experiments were further conducted, in which **BCX-Cu** (10 μM) was initially injected with various ions (60 μM) respectively, followed by adding equivalent amounts of Cu^{2+}. As a result, Fig. 5b showed the fluorescence intensity variations of **BCX-Cu** upon the addition of different co-existed ion species, which exhibited no significant changes compared to that obtained with Cu^{2+} alone, demonstrating the negligible effect of other co-existed metal ions to the fluorescence enhancement of **BCX-Cu** towards Cu^{2+}. The results further reveal the high selectivity of **BCX-Cu** towards varieties of competitive ions.

To promote further applications of **BCX-Cu**, the reaction kinetic behavior between the probe and Cu^{2+} in CH_3CN-H_2O (pH = 7.4, v / v, 1 / 1) was investigated by measuring fluorescence profiles of the free probe and probe with Cu^{2+} at different time. As can be seen from Fig. 6a, **BCX-Cu** showed a very weak and stable fluorescence intensity at ca. 570 nm under 503 nm excitation wavelength. By contrast, a prominent fluorescence intensity increase at 570 nm within the first 30 min can be observed upon treatment of Cu^{2+} (100 μM), which reached the peak value at 40 min and remained stable for 2 h, suggesting the end of the reaction between **BCX-Cu** and copper ions. Subsequently, the pH-dependent responses

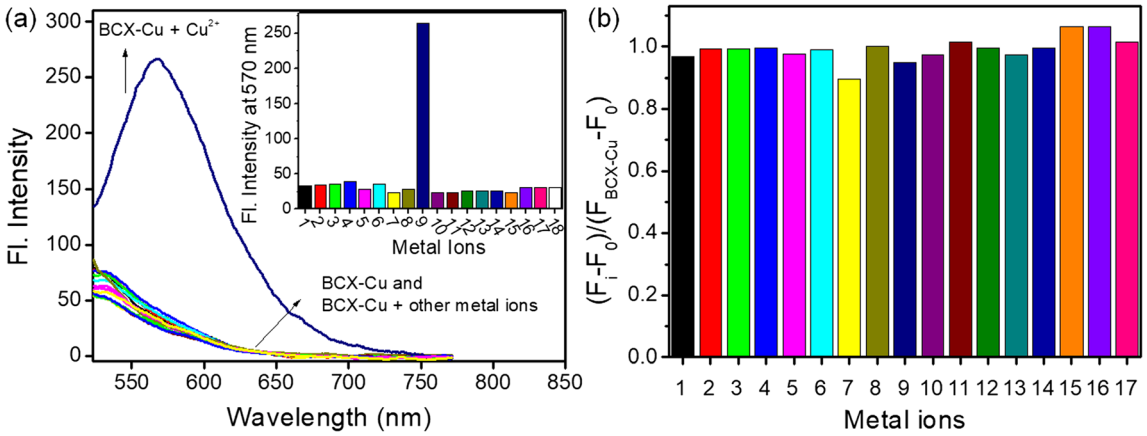

Fig. 5 **a** Fluorescence spectra of **BCX-Cu** (10 μM) with the addition of various cationic ions (60 μM) in CH_3CN-H_2O (pH = 7.4, v / v, 1 / 1). Inset: histograms represent the emission intensity of **BCX-Cu** (570 nm) with various ion species, 1–18 refer to: **BCX-Cu**, Ag^+, Al^{3+}, Ba^{2+}, Ca^{2+}, Co^{2+}, Cd^{2+}, Cr^{3+}, Cu^{2+}, Fe^{2+}, Fe^{3+}, Hg^{2+}, K^+, Mg^{2+}, Na^+, Ni^{2+}, Pb^{2+} and Zn^{2+}, respectively; **b** effects of co-existed metal ions (60 μM, 1–17: Ag^+; Al^{3+}; Ba^{2+}; Ca^{2+}; Co^{2+}; Cd^{2+}; Cr^{3+}; Cu^{2+} (only); Fe^{2+}; Fe^{3+}; Hg^{2+}; K^+; Mg^{2+}; Na^+; Ni^{2+}; Pb^{2+} and Zn^{2+}, respectively) on the emission intensity of **BCX-Cu** (10 μM) towards Cu^{2+} (60 μM) at 570 nm in CH_3CN-H_2O (pH = 7.4, v / v, 1 / 1). λ_{ex}: 500, slits: 10 nm, 10 nm

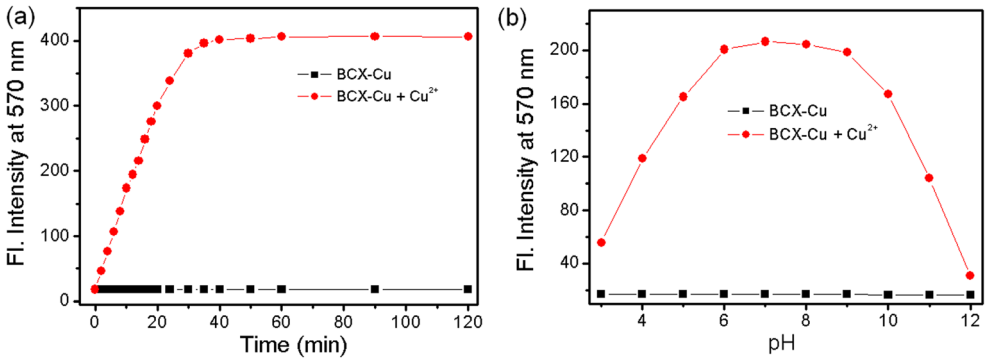

Fig. 6 **a** Fluorescence intensity (570 nm) of **BCX-Cu** alone (10 μM, black square) and upon treatment with Cu^{2+} (50 μM, red circle) at different time in CH_3CN-H_2O (pH = 7.4, v / v, 1 / 1). **b** Fluorescence intensity (570 nm) of **BCX-Cu** alone (10 μM, black square) and upon addition of Cu^{2+} (40 μM, red circle) in H_2O (v / v, 1 / 1) with different pH values. λ_{ex}: 503 nm, slits: 10 nm, 10 nm

of free **BCX-Cu** and **BCX-Cu** with Cu^{2+} were conducted under different pH conditions via fluorescence and absorbance spectra, respectively. Figure 6b exhibited no significant fluorescence change of **BCX-Cu** occurred between pH 3 and 12, which demonstrated the stability of the free probe over a wide pH region. In contrast, the presence of Cu^{2+} (4.0 equiv.) induced a gradually increase in fluorescence intensity from pH 3.0 to 6.0 compared to that of the probe alone, then remained nearly stable in the pH range between 6.0 and 9.0, which were corresponding to an efficient spirolactam ring opening structure caused by Cu^{2+}. However, an obvious decrease of the emission intensity appeared by varying pH values from 9.0 to 11.0. Meanwhile, the pH-dependent absorption spectra were also recorded and the results presented the same trend to those of evaluated through emission spectra (Fig. S9). The above results indicate **BCX-Cu** holds distinct performances to Cu^{2+} at pH from 6.0 to 9.0.

Fluorescence Imaging for Living Cells

In view of the desirable performances of the sensor **BCX-Cu** in sensitive and selective detection of Cu^{2+}, it was further utilized to monitor Cu^{2+} in living L929 cells by cell imaging. L929 cells were stained by **BCX-Cu** (3 μM) for 1 h at 37 °C, and rinsed with PBS to clear off excess **BCX-Cu**. As shown in Fig. 7, no obvious fluorescence was observed in the images of these cells

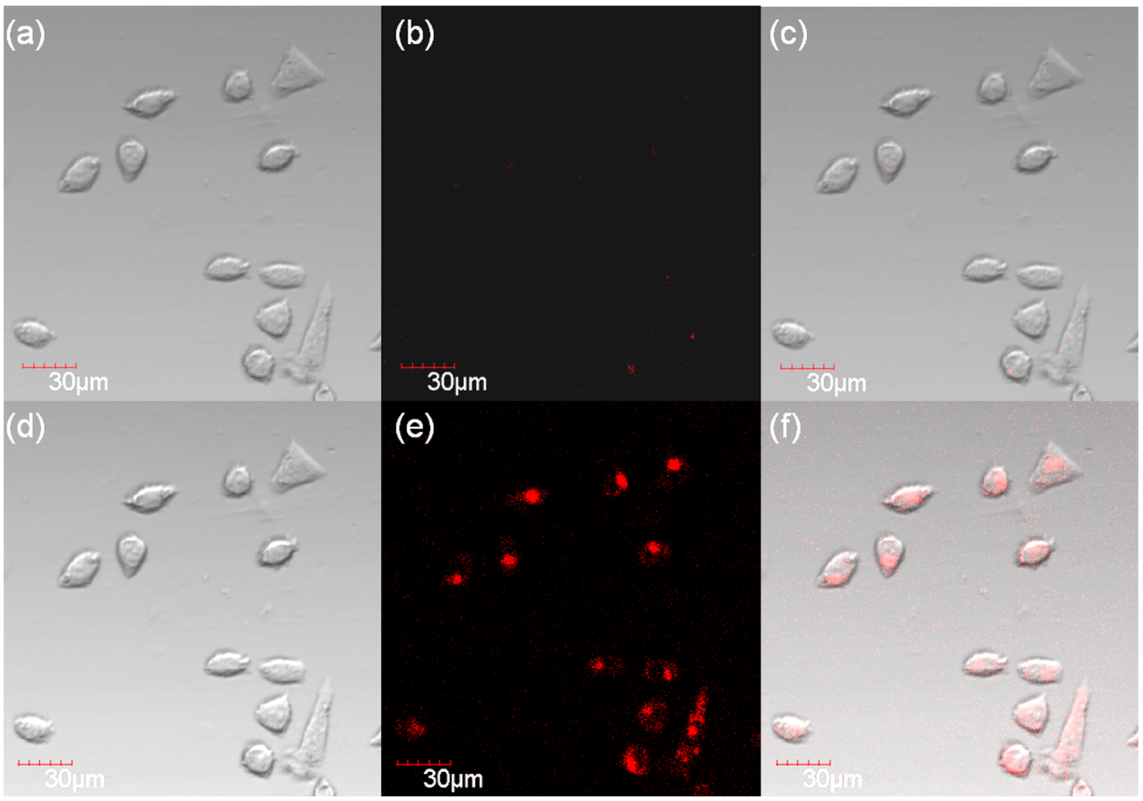

Fig. 7 Fluorescence images of **BCX-Cu** (3 μM) stained (1 h) L929 cells (top) and followed treatment of Cu^{2+} ions (18 μM) for 1 h (bottom). **a**, **d**: Bright field images, **b**, **e**: fluorescence images; **c**, **f**: emerged images. Images collected from the range of 520–610 nm upon 488 nm excitation

(520–610 nm) (Fig. 7a - c). Next, the cells were further incubated with Cu^{2+} (6.0 equiv.) for another 1 h. In contrast, the obvious fluorescence emission from the intracellular areas were observed (520–610 nm) (Fig. 7d - f). These results clearly indicate that **BCX-Cu** can penetrate the cell membrane and performs as a potential tracer for visualizing copper ions in living cells through fluorescent imaging technology.

Conclusion

In conclusion, a new biscarbazole-fused xanthene hybrid dye **MeBCX** has been prepared via the reactions of condensation and esterification, which exhibits stable optical signal in a wide pH range of 6–11 and a good cell membrane permeability. Taking advantage of the dye platform, we construct a fluorescent "off-on" probe **BCX-Cu** with selective and sensitive (LOD: 88.7 nM) response to Cu^{2+} via the specific cascade reaction of Cu^{2+}-induced spirolactam ring-opening and hydrolysis. In addition, **BCX-Cu** has been employed for detecting Cu^{2+} using L929 cells via fluorescence imaging, which indicates its living cell membrane permeability and promising applications for tracing Cu^{2+} in biological system.

Acknowledgements The authors thank the financial support of Doctoral Scientific Research Start-up Foundation of China West Normal University (18Q022), the National Natural Science Foundation of China (21671159), Meritocracy Research Funds of China West Normal University (17YC030) and Key Laboratory of Chemical Synthesis and Pollution Control of Sichuan Province (CSPC201802).

References

1. Domaille DW, Que EL, Chang CJ (2008) Synthetic fluorescent sensors for studying the cell biology of metals. Nat Chem Biol 4: 168–175
2. Ueno T, Nagano T (2011) Fluorescent probes for sensing and imaging. Nat Methods 8:642–645
3. Ni H, Wang Q, Jin L, Wang W, Dai L, Zhao C (2019) High selectivity and reversibility/reusability red emitting fluorescent probe for copper ions detection and imaging in living cells. J Lumin 206: 125–131
4. Ashton TD, Jolliffe KA, Pfeffer FM (2015) Luminescent probes for the bioimaging of small anionic species in vitro and in vivo. Chem Soc Rev 44:4547–4595
5. Huang K, He S, Zeng X (2017) A fluoran-based fluorescent probe via a strategy of blocking the intramolecular photoinduced electron transfer (PET) process. Tetrahedron Lett 58:2004–2008
6. Pang B, Li Q, Li C, Yang Z (2019) A highly selective and sensitive coumarin derived fluorescent probe for detecting Hg^{2+} in 100% aqueous solutions. J Lumin 205:446–450
7. Wałęsa-Chorab M, Skene WG (2017) Visible-to-NIR electrochromic device prepared from a thermally polymerizable electroactive organic monomer. ACS Appl Mater Interfaces 9: 21524–21531
8. Gotor R, Ashokkumar P, Hecht M, Keil K, Rurack K (2017) Optical pH sensor covering the range from pH 0-14 compatible with mobile-device readout and based on a set of rationally designed indicator dyes. Anal Chem 89:8437–8444
9. Li Z, Lv T, Zhang Y, Xu L, Zhang L, Wang X, Chen H, Guo Y (2018) A hematoporphyrin and indocyanine green co-delivery system with NIR triggered-controllable photoactivities for photodynamic therapy. Dyes Pigments 154:8–20
10. Li M, Long S, Kang Y, Guo L, Wang J, Fan J, Du J, Peng X (2018) De novo Design of phototheranostic sensitizers based on structure-inherent targeting for enhanced cancer ablation. J Am Chem Soc 140:15820–15826
11. Chen X, Pradhan T, Wang F, Kim JS, Yoon J (2011) Fluorescent chemosensors based on spiroring-opening of xanthenes and related derivatives. Chem Rev 112:1910–1956
12. Huang Y, Wang M, She M, Yang Z, Liu P, Li J, Shi Z (2014) Recent progress in the fluorescent probe based on spiro ring opening of xanthenes and related derivatives. Chin J Org Chem 34:1–25
13. Zheng H, Zhan XQ, Bian QN, Zhang XJ (2013) Advances in modifying fluorescein and rhodamine fluorophores as fluorescent chemosensors. Chem Commun 49:429–447
14. Kim HN, Lee MH, Kim HJ, Kim JS, Yoon J (2008) A new trend in rhodamine-based chemosensors: application of spirolactam ring-opening to sensing ions. Chem Soc Rev 37:1465–1472
15. Beija M, Afonso CAM, Martinho JMG (2009) Synthesis and applications of rhodamine derivatives as fluorescent probes. Chem Soc Rev 38:2410–2433
16. Sun YQ, Liu J, Lv X, Liu Y, Zhao Y, Guo W (2012) Rhodamine-inspired far-red to near-infrared dyes and their application as fluorescence probes. Angew Chem Int Ed 51:7634–7636
17. Wang Q, Jiao X, Liu C, Huang K, He S, Zhao L, Zeng X (2018) Novel π-extended hybrid xanthene dyes with two spirolactone rings for optoelectronic and biological applications. Org Biomol Chem 16:7609–7618
18. He S, Liu Q, Li Y, Wei F, Cai S, Lu Y, Zeng X (2014) Rhodamine 6G-based chemosensor for the visual detection of Cu2+ and fluorescent detection of Hg2+ in water. Chem Res Chin Univ 30(1):32–36
19. Lee D, Swamy KMK, Hong J, Lee S, Yoon J (2018) A rhodamine-based fluorescent probe for the detection of lysosomal pH changes in living cells. Sensors Actuators B Chem 266:416–421
20. Zhou L, Zhang X, Wang Q, Lv Y, Mao G, Luo A, Wu Y, Wu Y, Zhang J, Tan W (2014) Molecular engineering of a TBET-based two-photon fluorescent probe for ratiometric imaging of living cells and tissues. J Am Chem Soc 136:9838–9841
21. Feng XJ, Tian PZ, Xu Z, Chen SF, Wong MS (2013) Fluorescence-enhanced chemosensor for metal cation detection based on pyridine and carbazole. J Organomet Chem 78:11318–11325
22. Zhang J, Zhang L, Wei Y, Chao J, Wang S, Shuang S, Cai Z, Dong C (2013) A selective carbazole-based fluorescent probe for chromium (III). Anal Methods 5:5549–5554
23. Yang X, Zheng S, Bottger R, Chae HS, Tanaka T, Li S, Mochizuki A, Jabbour CE (2011) Efficient fluorescent deep-blue and hybrid white emitting devices based on carbazole/benzimidazole compound. J Phys Chem C 115:14347–14352
24. Palayangoda SS, Cai X, Adhikari RM, Neckers DC (2008) Carbazole-based donor - acceptor compounds: highly fluorescent organic nanoparticles. Org Lett 10:281–284
25. Jiao X, Xiao Z, Hui P, Liu C, Wang Q, Qiu X, He S, Zeng X, Zhao L (2019) A highly selective and pH-tolerance fluorescent probe for Cu^{2+} based on a novel carbazole-rhodamine hybrid dye. Dyes Pigments 160:633–640
26. Verwilst P, Sunwoo K, Kim JS (2015) The role of copper ions in pathophysiology and fluorescent sensors for the detection thereof. Chem Commun 51:5556–5571

27. Vonk WI, Wijmenga C, van de Sluis B (2008) Relevance of animal models for understanding mammalian copper homeostasis. Am J Clin Nutr 88:840s–845s
28. Muthaup G, Schlicksupp A, Hess L, Beher D, Ruppert T, Masters CL, Beyreuther K (1996) The amyloid precursor protein of Alzheimer's disease in the reduction of copper (II) to copper (I). Science 271:1406–1409
29. Strausak D, Mercer JF, Dieter HH, Stremmel W, Multhaup G (2001) Copper in disorders with neurological symptoms: Alzheimer's, Menkes, and Wilson diseases. Brain Res Bull 55: 175–185
30. Kaler SG (2011) ATP7A-related copper transport diseases-emerging concepts and future trends. Nat Rev Neurol 7:15–29
31. Gaggelli E, Kozlowski H, Valensin D, Valensin G (2006) Copper homeostasis and neurodegenerative disorders (Alzheimer's, prion, and Parkinson's diseases and amyotrophic lateral sclerosis). Chem Rev 106:1995–2004
32. Dujols V, Francis F, Czarnik AW (1997) A long-wavelength fluorescent chemodosimeter selective for Cu (II) ion in water. J Am Chem Soc 119:7386–7387
33. Sfrazzetto GT, Satriano C, Tomaselli GA, Rizzarelli E (2016) Synthetic fluorescent probes to map metallostasis and intracellular fate of zinc and copper. Coord Chem Rev 311:125–167
34. Cotruvo Jr JA, Aron AT, Ramos-Torres KM, Chang CJ (2015) Synthetic fluorescent probes for studying copper in biological systems. Chem Soc Rev 44:4400–4414
35. Huang K, Jiao X, Liu C, Wang Q, Qiu X, He S, Zhao L, Zeng X (2017) Synthesis of a novel π-extended hybrid rhodamine dye with far-red fluorescence emission and its application in bioimaging. Dyes Pigments 145:561–569
36. Huang K, Yue Y, Jiao X, Liu C, Wang Q, He S, Zhao L, Zeng X (2017) Fluorescence regulation of 4-aminobenzofluoran and its applications for Cu^{2+}-selective fluorescent probe and bioimaging. Dyes Pigments 143:379–386
37. Kempahanumakkagaari SK, Thippeswamy R, Malingappa P (2014) A new rhodamine B based fluorometric chemodosimeter for Cu^{2+} ion in aqueous and cellular media. J Lumin 146:11–17
38. Zheng X, Ji R, Cao X, Ge Y (2017) FRET-based ratiometric fluorescent probe for Cu^{2+} with a new indolizine fluorophore. Anal Chim Acta 978:48–54
39. Kumar M, Kumar N, Bhalla V, Sharma PR, Kaur T (2012) Highly selective fluorescence turn-on chemodosimeter based on rhodamine for nanomolar detection of copper ions. Org Lett 14:406–409
40. Chang LL, Gao Q, Liu S, Hu CC, Zhou WJ, Zheng MM (2018) Selective and differential detection of Hg^{2+} and Cu^{2+} with use of a single rhodamine hydrazone-type probe in the absence and presence of UV irradiation. Dyes Pigments 153:117–124
41. Yang Z, Zhao Y, Chen S, Bu Y, Zhu X, Du Y, Li F (2016) A highly sensitive and selective colorimetric "off-on" chemosensor for Cu^{2+} in aqueous media based on a rhodamine derivative bearing thiophene group. Sensors Actuators B Chem 235:414–419
42. Wu WN, Wu H, Zhong RB, Wang Y, Xu ZH, Zhao XL, Xu ZQ, Fan YC (2019) Ratiometric fluorescent probe based on pyrrole-modified rhodamine 6G hydrazone for the imaging of Cu^{2+} in lysosomes. Spectrochim Acta A Mol Biomol Spectrosc 212:121–127
43. Yuan Y, Sun S, Liu S, Song X, Peng X (2015) Highly sensitive and selective turn-on fluorescent probes for Cu^{2+} based on rhodamine B. J Mater Chem B 3:5261–5265
44. Shi Z, Tang X, Zhou X, Cheng J, Han Q, Zhou J, Wang B, Yang Y, Liu W, Bai D (2013) A highly selective fluorescence "turn-on" probe for Cu(II) based on reaction and its imaging in living cells. Inorg Chem 52:12668–12673
45. Yu C, Wang T, Xu K, Zhao J, Li M, Weng S, Zhang J (2013) Characterization of a highly Cu^{2+}-selective fluorescent probe derived from rhodamine B. Dyes Pigments 96:38–44
46. Tian MZ, Hu MM, Fan JL, Peng XJ, Wang JY, Sun SG, Zhang R (2013) Rhodamine-based 'turn-on'fluorescent probe for Cu (II) and its fluorescence imaging in living cells. Bioorg Med Chem Lett 23: 2916–2919
47. She M, Yang Z, Hao L, Wang Z, Luo T, Obst M, Liu P, Shen Y, Zhang S, Li J (2016) A novel approach to study the structure-property relationships and applications in living systems of modular Cu^{2+} fluorescent probes. Sci Rep 6:28972
48. Tang J, Ma S, Zhang D, Liu Y, Zhao Y, Ye Y (2016) Highly sensitive and fast responsive ratiometric fluorescent probe for Cu^{2+} based on a naphthalimide-rhodamine dyad and its application in living cell imaging. Sensors Actuators B Chem 236:109–115
49. Pu S, Ma L, Liu G, Ding H, Chen B (2015) A multiple switching diarylethene with a phenyl-linked rhodamine B unit and its application as chemosensor for Cu^{2+}. Dyes Pigments 113:70–77
50. Huang L, Chen F, Xi P, Xie G, Li Z, Shi Y, Xu M, Liu H, Ma Z, Bai D, Zeng Z (2011) A turn-on fluorescent chemosensor for Cu^{2+} in aqueous media and its application to bioimaging. Dyes Pigments 90:265–268
51. Hu ZQ, Wang XM, Feng YC, Ding L, Lu HY (2011) Sulfonyl rhodamine hydrazide: a sensitive and selective chromogenic and fluorescent chemodosimeter for copper ion in aqueous media. Dyes Pigments 88:257–261
52. Zhang B, Diao Q, Ma P, Liu X, Song D, Wang X (2016) A sensitive fluorescent probe for Cu^{2+} based on rhodamine B derivatives and its application to drinking water examination and living cells imaging. Sensors Actuators B Chem 225:579–585
53. Maity D, Karthigeyan D, Kundu TK, Govindaraju T (2013) FRET-based rational strategy for ratiometric detection of Cu^{2+} and live cell imaging. Sensors Actuators B Chem 176:831–837
54. Shivaprasad M, Govindaraju T (2011) Rhodamine based bright red colourimetric and turn-on fluorescence chemosensor for selective detection of Cu^{2+}. Mater Technol 26:168–172
55. Maity D, Govindaraju T (2011) Highly selective visible and near-IR sensing of Cu^{2+} based on Thiourea-Salicylaldehyde coordination in aqueous media. Chem Eur J 17:1410–1414
56. Liu C, Jiao X, He S, Zhao L, Zeng X (2017) A highly selective and sensitive fluorescent probe for Cu^{2+} based on a novel naphthalimide–rhodamine platform and its application in live cell imaging. Org Biomol Chem 15:3947–3954
57. Karstens T, Kobs KJ (1980) Rhodamine B and rhodamine 101 as reference substances for fluorescence quantum yield measurements. J Phys Chem 84:1871–1872
58. Gong YJ, Zhang XB, Mao GJ, Su L, Meng HM, Tan W, Feng S, Zhang G (2016) A unique approach toward near-infrared fluorescent probes for bioimaging with remarkably enhanced contrast. Chem Sci 7:2275–2285
59. Sibrian-Vazquez M, Escobedo JO, Lowry M, Fronczek FR, Strongin RM (2012) Field effects induce bathochromic shifts in xanthene dyes. J Am Chem Soc 134:10502–10508
60. Huang K, Jiao X, Liu C, Wang Q, Qiu X, Zheng D, He S, Zhao L, Zeng X (2017) Highly selective and sensitive fluorescent probe for mercury ions based on a novel rhodol-coumarin hybrid dye. Dyes Pigments 142:437–446
61. Pappayee N, Mishra AK (2000) Carbazole as an excited state proton transfer fluorescent probe for lipid bilayers in alkaline medium. Spectrochim Acta A Mol Biomol Spectrosc 56:1027–1034